Progress In Electromagnetics Research B, Vol. 47, 219–239, 2013

EXPERIMENTAL FIELD RECONSTRUCTION OF INCOHERENT SOURCES

Amedeo Capozzoli*, Claudio Curcio, and Angelo Liseno

Dipartimento di Ingegneria Biomedica, Elettronica e delle Telecomunicazioni, Università di Napoli Federico II, via Claudio 21, Napoli I 80125, Italy

Abstract—The problem of characterizing random sources from near-field measurements and of devising the random field sampling procedure is tackled by a stochastic approach. The presented technique is an extension of that introduced in [22] and successfully adopted to experimentally characterize deterministic (CW and multi-frequency) radiators and fields. Under the assumption that the source is wide sense stationary, quasi-monochromatic and incoherent, its intensity is reconstructed by time-domain field measurements aimed at extracting information from the mutual coherence of the acquired near-field. The linear relation between the field coherence and the source intensity is inverted by using the Singular Value Decomposition (SVD) approach, properly representing the source intensity distribution by exploiting the a priori information (e.g., its size and shape) on the radiator. The sampling of the radiated random field is devised by a singular value optimization procedure of the relevant finite dimensional linear operator. Experimental results using a slotted reverberation chamber as incoherent source assess the performance of the approach.

1. INTRODUCTION

The purpose of radiated field emission and immunity measurements is to ensure the Electromagnetic Compatibility (EMC) of different devices located in complex environments, such as office rooms, factory floors, or aircraft hulls, or between different components of very large scale integration circuits generating Electromagnetic Interference (EMI) problems [1]. Examples concern, but are not limited to,

- EMI problems of computers, peripherals and data cables [2];

Received 25 July 2012, Accepted 19 December 2012, Scheduled 2 January 2013

* Corresponding author: Amedeo Capozzoli (a.capozzoli@unina.it).

- electromagnetic shielding for the protection of electronic equipment and systems against EMI for which apertures, needed for cable interconnections or cooling, can degrade the shielding efficiency [3];
- the operation of automotive electronics which is ceaselessly undergoing a dramatic increase in clock speed translating into potentially greater interferences [4];
- switched mode power supplies, typically used to feed integrated electronic devices and power drive systems and for which knowing the radiated near-field helps the correct EMC design of the device [5, 6];
- the design of high-speed Printed Circuit Boards (PCB), for which the proximity of various components may sometimes render the design completely unoperational [7].

In this framework, a standard EMC measurement problem is to determine the radiation/immunity characteristics of unintentional sources.

Traditional emission and immunity measurements implicitly assume that the equipment under test (EUT) has a simple dipole-like radiation and reception pattern. When this is true, reverberation chambers [8] or Transverse Electromagnetic (TEM) cells [9] can be used for total radiated power measurements or to determine the complex dipole moments (electric and magnetic) of the source, respectively.

However, as the EUT becomes electrically large, it can be expected to have complex emission/reception patterns, especially as the frequency raises to the GHz range. In these circumstances, the directivity of the EUT [10] becomes an important factor determining the coupling between the different involved devices.

Unfortunately, measurements in a reverberation chamber or a TEM cell determine the total radiated/received power, but not the electromagnetic field at any particular point in space. Thus, simply applying traditional test procedures does not allow to obtain a full picture of the EUT immunity/emissions.

Near-Field (NF) measurements [11–13] are being recognized to be very useful in characterizing the EMC of industrial, active, or passive circuits, as witnessed by the current interest of several research laboratories in the development of near-field scanners for the study of chip-level electromagnetic compatibility [14–16] and by commercial availability of automatic measurement systems to identify "hot spots" of PCB currents [17].

NF techniques consist of calculating, from NF data measured in the vicinity of the EUT, the radiated field at desired points in

space [18, 19], and, in particular, at the distances of 10 to 30 meters from the EUT as required by standard EMC regulations. They permit the reduction of the high costs related to large anechoic or semi-anechoic chambers or of large outdoor test ranges. However, performing NF measurements to achieve the full EUT pattern is time consuming and can appear unsuited for routine EMC test purposes, unless the number of measurements can be strictly limited, and adjusted, according to the degree of complexity of the EUT. Unfortunately, standard NF techniques do not provide sampling criteria to reduce the overall number of needed field samples.

NF techniques are currently widely used to reconstruct the amplitude and phase of deterministic (Continuous Wave — CW — or multi-frequency) fields radiated by antennas or scatterers [20]. In this framework, the Authors have recently proposed in [21, 22] a particularly efficient field sampling strategy.

In contrast to antenna characterization, in many EMC cases, fields produced by unintentional sources or by intentional sources for which the temporal evolution cannot be foreseen deterministically, but rather stocastically [23], are involved. When the emissions are random, conventional deterministic complex (amplitude and phase) and phaseless NF techniques cannot be straightforwardly applied. Indeed, frequency-domain approaches are not suited due to the randomness of the field phase [20]. Moreover, to use time-domain techniques [24], the signals should be simultaneously measured at every sampling point of the measurement domain to evaluate the necessary field correlations, leading to an impractically burdened measurement setup. Finally, the existing near-field phaseless approaches [25] require proper extensions to be successfully adopted for the case of stochastic sources.

Recently, a NF technique based on the processing of the coherence function of narrow-band fields radiated by an EUT has been proposed [23] and experimentally validated [26] to characterize the radiation by a GSM telephone handset. In such a technique, the EUT is modeled as a superposition of narrow-band uncorrelated elementary sources and the radiated field is regarded as a weakly stationary stochastic process in time and space. The coherence function of the fields is related to the intensity of the source which, in turn, is recovered by a Singular Value Decomposition (SVD) approach. Unfortunately, the technique in [23, 26] does not point out a sampling strategy.

In this paper, the problem of reconstructing random sources from NF measurements is tackled and a strategy to effectively perform the random field sampling [27] is devised by a proper stochastic approach. The presented technique is an extension of that introduced

in [21, 22] and successfully adopted to experimentally characterize deterministic (CW-multifrequency) radiators and fields [19]. Under the assumption that the source is wide sense stationary [28] and quasi-monochromatic [29], its second order statistics can be reconstructed by time-domain NF field measurements aimed at forming the mutual coherence of the measured field itself [30]. The linear relation between the coherence of the NF and the second order statistics of the source can be inverted by using the SVD [31] approach, properly representing the source statistics by exploiting the a priori information (e.g., its size and shape) available on the radiator. Finally, the sampling of the random NF field is performed by a singular value optimization procedure of the relevant linear operator.

The performance of the approach is analyzed in a 2D scalar radiation geometry involving plane and parallel source and observation domains and incoherent [32, 33] radiators. For such a problem, preliminary results have been presented in [30]. Here, we illustrate experimental results aimed at showing how the approach is capable to correctly reconstruct the intensity distribution of random radiators with a number of measurements which is significantly smaller than those required by more "standard" techniques, as it has been already proven in the CW, multi-frequency or narrow-band cases [21, 22, 30]. In this paper, random incoherent sources have been produced by properly slotting one of the walls of a reverberation chamber with one or more narrow apertures.

The paper is organized as follows. In Section 2, the problem is formulated and, under the hypothesis of narrow-band, wide-sense stationary and incoherent sources, the coherence function of the NF is related to the source intensity distribution (van Cittert-Zernike theorem), thus obtaining the relevant, linear unknown-to-data relationship to be inverted for the reconstruction of the unknown random sources. In Section 3, the problem discretization is introduced when the incoherent source intensity distribution is represented by means of Prolate Spheroidal Wave Functions (PSWFs) [34, 35], and the solution scheme employing the SVD approach is indicated. Section 4 is devoted to describe the singular value optimization procedure to define the number and positions of the field samples. Finally, Section 5 presents numerical and experimental results.

2. FORMULATION OF THE PROBLEM

Let us consider for the sake of simplicity, but without any loss of generality, the 2D scalar radiation problem of an intentional or unintentional time-domain strip source, of size $2a'$, according to the

geometry in Fig. 1. We define $\underline{j}_s(x',t) = j_s(x',t)\hat{i}_y$ as the strip source, having support on $(-a', a')$, which can be thought of as being obtained from a single current formulation of the equivalence theorem applied to the $z < 0$ half-space filled with a perfect magnetic conductor [36, 37]. We assume that the background medium is free-space and consider an ideal probe acquiring the y component e of the radiated field. Without any loss of generality, we suppose, just to clarify things, to collect the field on the segment $(-a, a)$, parallel and centered to the source and located at a distance d apart from it, at a number M of sampling positions (x_m, d). For remarks on the non-ideality of the probe and on different descriptions of the source radiation, see [21]. The radiating source is assumed to be quasi-monochromatic, with spectrum centered around the frequency f_0 and with bandwidth $\Delta f \ll f_0$ [29]. This hypothesis is not a limitation since, in practice, the radiated spectrum of many intentional or unintentional sources is narrowband [2]. Accordingly, also the radiated field is quasi-monochromatic.

Henceforth, complex analytic signal representations are used for sources and fields, namely [29]:

$$u(P,t) = \int_0^\infty U(P,f)e^{j2\pi ft}df \tag{1}$$

where u can be either j_s or e. U is its Fourier transform and j the imaginary unit.

If we further assume that the distance $R = \sqrt{(x-x')^2 + d^2}$ between a generic source point $(x', 0)$ and a generic observation point

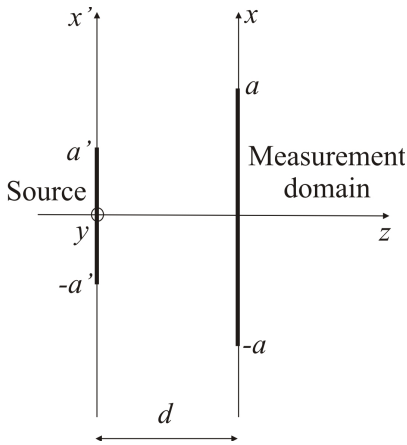

Figure 1. Geometry of the problem.

(x, d) satisfies $R\Delta\beta \ll 1$ with $\Delta\beta = 2\pi\Delta f/c$, c being the free-space light speed, then the relation between j_s and e can be written as [29]

$$e(x,t) = -\frac{\omega_o \mu}{4} \int_{-a'}^{a'} H_0^{(2)}(\beta_0 R) j_s(x',t) dx' \tag{2}$$

where $H_0^{(2)}$ is the Hankel function of zero-th order and second kind, $\omega_0 = 2\pi f_0$, $\beta_0 = \omega_0/c$, and $-(\omega_0\mu/4)H_0^{(2)}(\beta R)$ is the relevant, frequency-domain, 2D scalar Green's function [38].

In order to determine a relation between the mutual coherences of source and field, we assume that j_s is wide sense stationary, so that its mutual coherence function can be expressed as [23]

$$\Gamma_{j_s}\left(x', x'', \tau\right) = \left\langle j_s(x',t') j_s^*\left(x'', t'-\tau\right)\right\rangle \simeq \Gamma_{j_s}\left(x', x'', 0\right) e^{-j2\pi f_0 \tau}, \tag{3}$$

where $\langle\cdot\rangle$ denotes an average over the ensemble of source realizations, which can be computed as a time average under the hypothesis of ergodicity [30, 32]. Accordingly, the field is wide sense stationary and its mutual coherence function $\Gamma_e(x_1, x_2, \tau)$ can be expressed as

$$\begin{aligned}\Gamma_e(x_1, x_2, \tau) \simeq & \left(\frac{\omega_0\mu}{4}\right)^2 \int_{-a'}^{a'} \int_{-a'}^{a'} H_0^{(2)}(\beta_0 R_1) \\ & \times H_0^{(2)^*}(\beta_0 R_2) \Gamma_{j_s}\left(x', x''\right) dx' dx'' e^{-j2\pi f_0 \tau},\end{aligned} \tag{4}$$

where, with an abuse of notation, we have set $\Gamma_{j_s}(x', x'') = \Gamma_{j_s}(x', x'', 0)$, and $R_1 = \sqrt{(x_1 - x')^2 + d^2}$, $R_2 = \sqrt{(x_2 - x'')^2 + d^2}$.

By setting $\tau = 0$, then the equation

$$\begin{aligned}\Gamma_e(x_1, x_2) \simeq & \left(\frac{\omega_0\mu}{4}\right)^2 \int_{-a'}^{a'} \int_{-a'}^{a'} H_0^{(2)}(\beta_0 R_1) \\ & \times H_0^{(2)^*}(\beta_0 R_2) \Gamma_{j_s}\left(x', x''\right) dx' dx'',\end{aligned} \tag{5}$$

where, again with an abuse of notation, $\Gamma_e(x_1, x_2) = \Gamma_e(x_1, x_2, 0)$, defines the inverse source problem for partially coherent sources and fields [23, 28, 33, 39], and, in particular, that of deducing second order statistics of the source from second order statistics of the radiated field on the segment $(-a, a)$ of the $z = d$ axis. As known, not only in the case of coherent sources, but also when partially coherent radiators are involved, this problem has a nonunique solution [40].

Uniqueness can be restored when referring to incoherent (i.e., delta correlated sources) or quasi-homogeneous sources [28, 33, 39]. In the case of incoherent sources, namely, the case of interest in the present paper, $\Gamma_{j_s}(x', x'') = I(x')\delta(x' - x'')$, so that Eq. (5) can be rewritten as

$$\Gamma_e(x_1, x_2) \simeq \left(\frac{\omega_0\mu}{4}\right)^2 \int_{-a'}^{a'} H_0^{(2)}(\beta_0 R_1) H_0^{(2)^*}(\beta_0 R_2) I(x') dx' \tag{6}$$

where now $R_1 = \sqrt{(x_1 - x')^2 + d^2}$, $R_2 = \sqrt{(x_2 - x')^2 + d^2}$. Eq. (6) is an expression of the van Cittert-Zernike theorem [32].

3. RECONSTRUCTION OF INCOHERENT SOURCES

In order to solve the inverse source problem defined by Eq. (6), let us first discuss a finite dimensional representation of I. To this end, as a priori information on the source, besides the incoherency, we assume to know the spatial support $(-a', a')$ of j_s. Then, following [21, 41], j_s can be expanded as

$$j_s(x', t) = \sum_{p=1}^{P} \sum_{k=1}^{K} f_{pk} d_p(t) \psi_k[x', \beta_0 a'] e^{-j2\pi f_0 t}, \tag{7}$$

where the $\psi_k[\cdot, \beta_0 a']$'s are the Prolate Spheroidal Wave Functions (PSWFs) with space-bandwidth product $\beta_0 a'$ [34, 35], $K = [(2/\pi)\beta_0 a']$, the symbol $[\cdot]$ denoting the integer part. The d_p's are slowly varying functions of $\mathcal{L}^2(0, T)$, $(0, T)$ being the observation time [41], expanding the baseband part of $j_s(x', t)$, and the f_{pk}'s are expansion coefficients. Accordingly, the behavior of $H_0^{(2)}(\cdot)$ against the x' variable in Eq. (2) can be described by the above mentioned K PSWFs, so that the Hankel functions appearing in Eq. (6) can be approximately represented as

$$H_0^{(2)}(\beta_0 R_i) \simeq \sum_{k=1}^{K} a_k(x_i) \psi_k \left[x', \beta_0 a'\right], \qquad i = 1, 2 \tag{8}$$

where the a_k's are proper expansion functions whose expression is left unspecified, being irrelevant for our reasoning. Consequently,

$$\begin{aligned} \Gamma_e(x_1, x_2) \simeq & \left(\frac{\omega_0 \mu}{4}\right)^2 \sum_{k'=1}^{K} \sum_{k''=1}^{K} a_{k'}(x_1) a_{k''}^*(x_2) \\ & \times \int_{-a'}^{a'} \psi_{k'} \left[x', \beta_0 a'\right] \psi_{k''} \left[x', \beta_0 a'\right] I(x') dx'. \end{aligned} \tag{9}$$

From Eq. (9), it can be deduced that only the components of I on the space spanned by the products of functions $\psi_{k'}(x')\psi_{k''}(x')$'s have a significant image on the field coherence $\Gamma_e(x_1, x_2)$. Furthermore, the functions $\psi_{k'}(x')\psi_{k''}(x')$'s approximately span the space of PSWFs with space-bandwidth product $2\beta_0 a'$. Therefore, we set

$$I\left(x'\right) = \sum_{k=1}^{2K} I_k \psi_k \left[x', 2\beta_0 a'\right], \tag{10}$$

where $\psi_k[x', 2\beta_0 a']$ is the k-th PSWFs with space bandwidth product $2\beta_0 a'$. It should be noted that the PWSFs are real functions, which is a convenient property when expanding the real function I.

Taking now into account that e is sampled at a number M of points $\{x_m\}_{m=1}^{M}$ on the segment $(-a, a)$, so that $M \times M$ values of Γ_e are obtained, then Eq. (6) can be recast as

$$\underline{V} = \underline{\underline{Z}}\, \underline{I} \tag{11}$$

where $\underline{V}$ is the column vector containing the values of the $\Gamma_e(x_m, x_n)$ of the mutual coherence at (x_m, d) and (x_n, d), and $\underline{I}$ is the vector containing the b_k's. The elements $Z_{mn;k}$ of the matrix $\underline{\underline{Z}}$ are

$$\left(\frac{\omega_0 \mu}{4}\right)^2 \int_{-a'}^{a'} H_0^{(2)}(\beta_0 R_{1_m}) H_0^{(2)^*}(\beta_0 R_{2_n}) \psi_k \left[x', 2\beta_0 a'\right] dx', \tag{12}$$

where now $R_{1_m} = \sqrt{(x_m - x')^2 + d^2}$, $R_{2_n} = \sqrt{(x_n - x')^2 + d^2}$. For the matrix $\underline{\underline{Z}}$, one index has been substituted in place of the couples of indices (m, n) according to a convenient mapping.

For fixed sample number M and locations, the characterization of the incoherent source amounts at determining the source intensity I in terms of the expansion coefficients $\underline{I}$. Unfortunately, the inversion of Eq. (11) is affected by ill-conditioning, so that a regularized approach should be exploited. A possible solution is provided by the use of the Truncated Singular Value Decomposition (TSVD) approach [42], even if other regularization strategies are possible [43].

4. OPTIMAL SAMPLE NUMBER AND LOCATIONS

According to the theory of the SVD approach, to reliably and accurately retrieve the subspace components of the source intensity, the matrix $\underline{\underline{Z}}$ should have the best possible conditioning [19, 21, 22]. On the other hand, $\underline{\underline{Z}}$ is not univocally defined, since it depends on the choice of both M, the number of sampling points, and the sample distribution. In other words, we have at our disposal a family of matrices $\underline{\underline{Z}}$ with different behaviors of the singular values. Therefore, the inversion should be performed by exploiting the element of the family with "the most convenient" singular value behavior. To cope with this point, the solution of the linear inverse problem (11) should then be preceded by an optimization step leading to the best choice of both M and the sample locations [19, 21].

This particularly flexible approach enables working out here, rigorously and for the very first time, the field sampling in the incoherent case and can be used to derive the field sampling also in

the partially coherent case, when the source statistics are known (e.g., [28]).

Let us then denote the singular values of $\underline{\underline{Z}}$ by σ_t, with $t = 1, \ldots, T$ and $T = \min\{M \times N, K\}$. The behavior of the σ_t's affects the amount of information conveyed on $\underline{I}$ by $\underline{V}$ [44]. Accordingly, among all the possible matrices $\underline{\underline{Z}}$ and for a fixed M, it is convenient to choose the locations of the sampling points providing the "flattest" singular values behavior. This choice can be accomplished, for a fixed M, by maximizing for instance the functional [19, 21]

$$\Phi = \sum_{t=1}^{T} \frac{\sigma_t}{\sigma_1} \tag{13}$$

evaluating the "area" subtended by the normalized singular values σ_t/σ_1.

Concerning now the choice of the "optimal" number of samples M, since Φ admits a meaningful interpretation in terms of generalized Shannon number [44], then, on denoting by $\Phi_{opt}(M)$ the maximum of Φ for a given M, we expect that adding further sampling points to the segment $(-a, a)$ of the $z = d$ axis (i.e., increasing M) will increase $\Phi_{opt}(M)$ until the maximum amount of information which can be gathered from such a domain is reached. Beyond this condition, no further information can be conveyed on $\underline{I}$ by any newly added field sample. Since $\underline{I}$ belongs to a finite dimensional space, this will correspond to the appearance of very small singular values and thus to a "saturation" behavior of $\Phi_{opt}(M)$ against M [19, 21], making the lastly added samples irrelevant. The number M at the saturation knee represents the minimum number of samples needed to achieve all the information available on $\underline{I}$ from the mentioned segment $(-a, a)$.

Finally, to mitigate the trapping problem when optimizing Φ and to improve the efficiency of the procedure, a representation of the sampling points by properly chosen expansion functions is adopted [19, 21] to reduce the number of parameters to be determined and to allow the progressive enlargement of the unknowns. In other words, the abscissas x_m's are represented as

$$x_m = \sum_{l=0}^{L-1} c_l P_l(\xi_m), \qquad m = 1, \ldots, M \tag{14}$$

where the ξ_m's are uniformly spaced within $[-1, 1]$, the P_l's are basis functions, and the c_l's are the expansion coefficients. By Eq. (14), a set of M uniformly spaced abscissas ξ_m's is mapped into a set of M nonuniformly spaced abscissas x_m in such a way that only the few c_l's are the parameters to be optimized. The number L of parameters c_l

is unrelated to the number of sampling points and could be arbitrarily chosen so that the number of basis functions P_l's (which can be progressively enlarged) can be chosen to allow a significant reduction of the number of unknowns to be determined while optimizing Φ, with beneficial effects on the computational burden of the search algorithm. Since the local sampling step of the field is expected to smoothly change from point to point, a polynomial (e.g., Legendre) expansion involving few (three or four) terms is generally sufficient to provide an adequate representation of the x_m's.

5. NUMERICAL AND EXPERIMENTAL RESULTS

In this section, we show the results of a numerical and experimental analysis performed to assess the performance of the developed approach.

The experiments have been carried out within the anechoic chamber available at the Dipartimento di Ingegneria Biomedica, Elettronica e delle Telecomunicazioni (DIBET) of the Università di Napoli Federico II. A reverberation chamber has been exploited to obtain incoherent sources [45] since, as known, the coherency length of the reverberating field is of the order of $\lambda/2$ [46]. The reverberation chamber, already available at DIBET, is made up by a cubic cavity with side equal to 0.5 m and equipped by three metallic fan-shaped stirrers (see Fig. 2). It is fed by a rectangular waveguide operating in the Ku band and one of its side is removable and replaceable with slotted metallic panels. For our purposes, two removable panels have been employed, one with a slot, 0.5 cm $\times$ 30 cm sized and one with

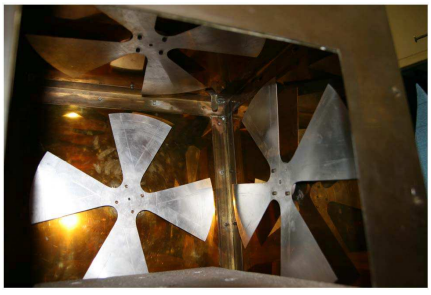

Figure 2. Illustration of the interior of the reverberating chamber and of the fan-shaped stirrers.

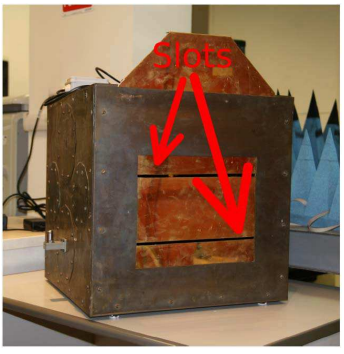

Figure 3. The reverberating chamber with the two-slots panel and the feeding input.

two slots, each 0.5 cm × 30 cm sized and reciprocally separated by a distance of 14 cm (see Fig. 3 as well as Fig. 4 for the reciprocal arrangement of the slots and the source region). Such a distance has been chosen so to guarantee the incoherency of the fields excited between the slots. Furthermore, the elongated shape of the slots as well as their orientation along the y axis, orthogonal to both the investigation domain $(-a', a')$ and the observation domain $(-a, a)$, have been selected to meet the assumption of a 2D geometry.

A probe acquires the field radiated by the slots by occupying, one after the other and thanks to a positioner, the desired sampling points, according to the geometry of Fig. 1 (see also Fig. 5). As probe, a truncated rectangular waveguide has been adopted. Being the probe electrically small, probe correction is not very relevant [47]. When necessary, probe compensation can be performed for the presented approach according to the same guidelines in [48].

The data have been acquired by a Vector Network Analyzer (VNA) Anritsu 37397C, working in the 40 MHz–65 GHz frequency band, which also provides the feeding of the reverberation chamber. More in detail, the data have been acquired in the 14 GHz–16 GHz band. We underline that emission measurements for the EMC check of device must be carried out, according to the standards [49], in the frequency domain by sweeping in frequency and measuring the emissions at each frequency. The signals recorded for each sampling point have been then transformed in the time domain so to work out an estimate of the coherence matrix under the hypothesis of ergodicity [30, 32].

In the following, we report the results of the experimental analysis.

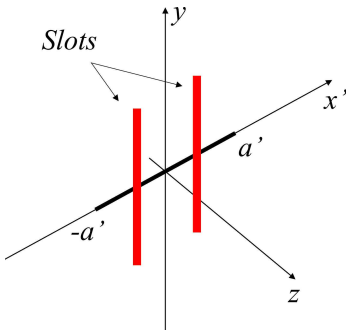

Figure 4. Reciprocal arrangement of the slots and the investigation region.

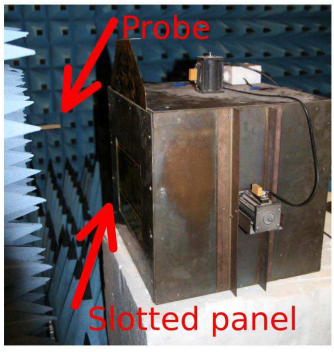

Figure 5. The reverberating chamber with the measurement probe.

5.1. Uniform Sampling — Single Slot

The first example regards the case of a single slot when the data are acquired with an uniform sampling step equal to $\lambda_0/5$, λ_0 being the wavelength at the center frequency of 15 GHz.

The size of the investigation and of the observation domains have been $2a' = 22\,\text{cm}$ and $2a = 20\,\text{cm}$, respectively, whereas their reciprocal distance has been $d = 15.5\,\text{cm}$. The total number of measurement points has been 51.

Figure 6 illustrates the singular values behavior for the considered case (blue starred line). As it can be seen, all the 22 singular values are relevant, meaning that all the considered unknown coefficients I_k's can be inverted. It should be also noticed that the number

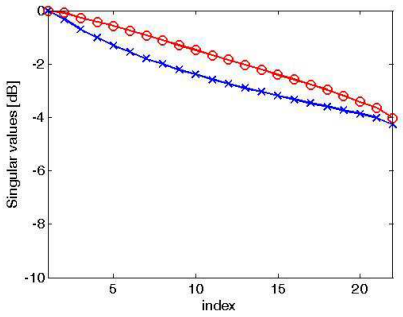

Figure 6. Singular values distribution for the uniform (blue starred line) and nonuniform (red circled line) cases.

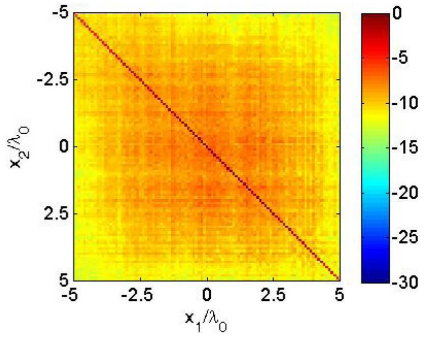

Figure 7. Amplitude distribution of $\Gamma_e(x_1, x_2)$ for the case of a single slot.

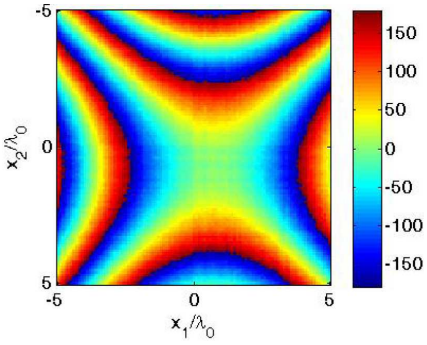

Figure 8. Phase distribution of $\Gamma_e(x_1, x_2)$ for the case of a single slot.

of relevant singular values is significantly lower than the number of uniform sampling points.

Figures 7 and 8 show the amplitude and phase, respectively, of $\Gamma_e(x_1, x_2)$. From the fringes of the phase distribution of $\Gamma_e(x_1, x_2)$ the presence of the single radiator could be already deduced. This is confirmed by the reconstruction shown in Fig. 9, whose peak clearly singles out the position of the slot. Finally, Fig. 10 illustrates the result obtained if the data are processed according to the coherent radiation model of Ref. [21]. More in detail, to obtain the reconstruction in Fig. 10, only the data at $f = f_0$ have been considered. As it can be seen, the reconstruction is meaningless, thus pointing out the need of

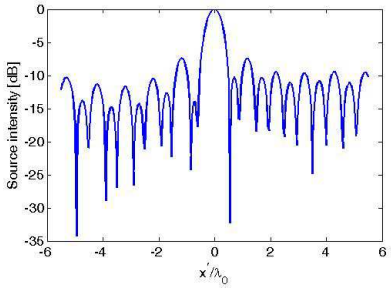

Figure 9. Single slot: reconstruction of the intensity distribution.

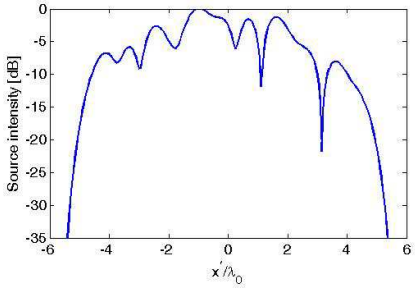

Figure 10. Single slot: reconstruction of the intensity distribution by using the same "coherent" processing as in [21].

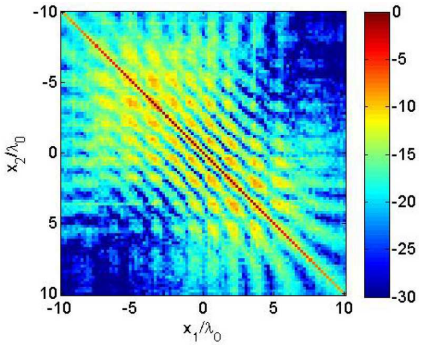

Figure 11. Amplitude distribution of $\Gamma_e(x_1, x_2)$ for the case of a double slot with uniform sampling.

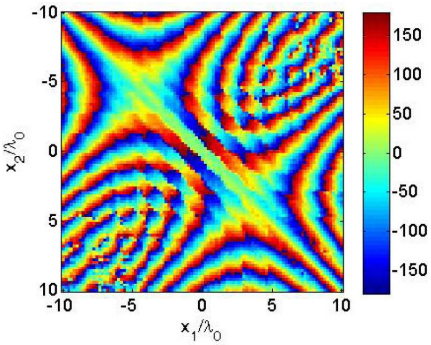

Figure 12. Phase distribution of $\Gamma_e(x_1, x_2)$ for the case of a double slot with uniform sampling.

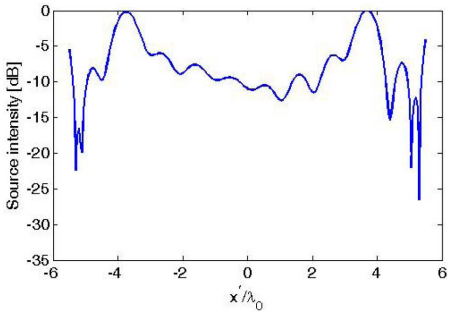

Figure 13. Double slot and uniform sampling: reconstruction of the intensity distribution.

adopting the proposed processing based on the incoherent modelling of the source.

5.2. Uniform Sampling — Double Slot

The second example regards the case of a double slot, still addressed under a uniform sampling of the radiated field. The size of the investigation region is the same as that for the foregoing case, whereas the observation domain now corresponds to $2a = 40\,\text{cm}$.

Figures 11 and 12 display the amplitude and phase, respectively, of $\Gamma_e(x_1, x_2)$. Once again, from the fringes of the phase distribution of $\Gamma_e(x_1, x_2)$, the presence of the two radiators could be already deduced. This is confirmed by the reconstruction shown in Fig. 13 whose maxima clearly spot out the slot positions.

5.3. Nonuniform Sampling — Two Slots

We finally show the case of a double slot when the radiated field is acquired by a non-uniform sampling. The investigation domain is again $2a' = 22\,\text{cm}$ sized, whereas the observation domain is such that $2a = 60\,\text{cm}$. Figs. 14 and 15 show the non-uniform sampling points determined following the procedure in Section 4 and the uniform sampling exploited in the foregoing subsections, respectively. As it can be seen, the number of sampling points is now 22, which is much less than the number of 51 sampling points involved in the two previous cases which, nevertheless, corresponded to even narrower observation regions.

Figure 6 depicts the singular values behavior for the considered test case (red circled line). As it can be appreciated, again all the 22 singular values are relevant. Furthermore, such a behavior is

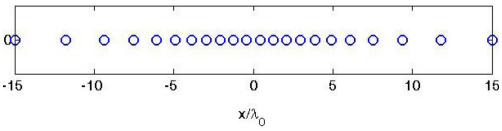

Figure 14. Sampling point locations for the case of a double slot with non-uniform sampling.

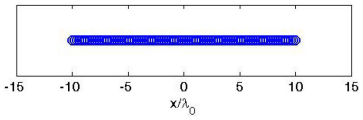

Figure 15. Sampling point locations for the case of a single and double slot with uniform sampling.

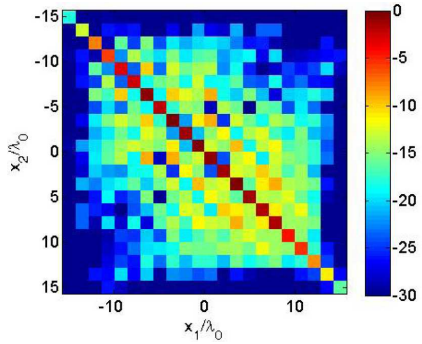

Figure 16. Amplitude distribution of $\Gamma_e(x_1, x_2)$ for the case of a double slot with non-uniform sampling.

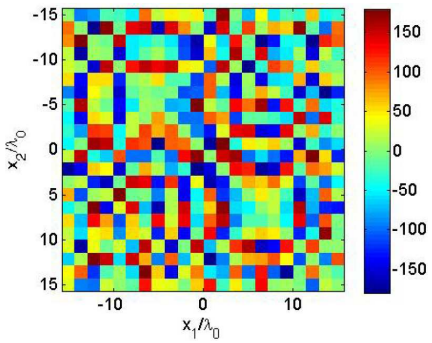

Figure 17. Phase distribution of $\Gamma_e(x_1, x_2)$ for the case of a double slot with non-uniform sampling.

close to that concerning the uniform sampling, with the advantage now that the number of involved samples is, as mentioned, much lower. The closeness of the two behaviors can be expected since, in a comparable measurement region, the uniform sampling corresponds to a significantly narrower sampling step.

Figures 16 and 17 illustrate amplitude and phase, respectively, of $\Gamma_e(x_1, x_2)$, whereas Fig. 18 depicts the reconstructed source intensity distribution.

Finally, Fig. 19 shows the same reconstructions of the two slots as in Figs. 13 and 18, obtained under the same uniform and non-uniform measurement configurations, but when model-based numerical data are considered. As it can be seen, the uniform and non-uniform approaches have similar performance, the latter exploiting a significantly lower number of measurements. It should be moreover mentioned that mismatches between the model considered for the coherence in Eq. (6) and the actual one affect the reconstructions by

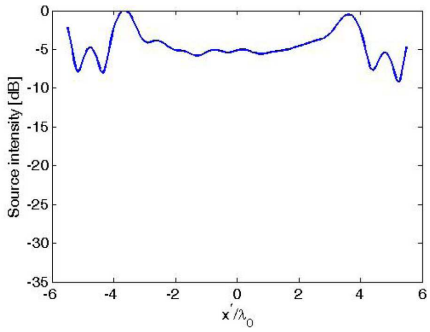

Figure 18. Double slot and nonuniform sampling: reconstruction of the intensity distribution.

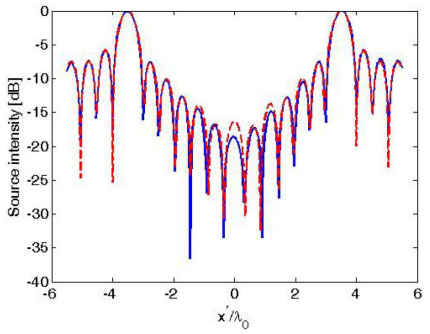

Figure 19. Double slot and uniform (red dashed line) and nonuniform (blue solid line) sampling with numerical data: reconstruction of the intensity distribution.

both the approaches using uniform and nonuniform sampling points. Such mismatches affect also the procedure for determining the sample locations, and so the "optimality" of the nonuniform sampling points, for the nonuniform approach only. Accordingly, the slight differences in the dynamics of the two reconstructions in Figs. 13 and 18 should be ascribed to slight model mismatches.

6. CONCLUSIONS AND FUTURE DEVELOPMENTS

An approach has been presented to the problem of characterizing random sources from NF measurements. The attention has been focused on the case of incoherent sources under a scalar, 2D geometry.

The source intensity has been properly represented by PSWFs, exploiting the a priori knowledge on the extent of the source, while the NF has been acquired at nonuniformly distributed sample locations maximizing the amount of information extracted from the measurement domain to accurately determining the unknown source. The sample locations have been chosen according to a singular value optimization procedure. The source reconstruction problem has been then solved by a TSVD approach.

Experimental results, employing a slotted reverberation chamber as incoherent source of radiation, have been presented assessing the performance of the method.

It has been shown that the approach is capable to significantly

reducing the number of the required field samples as compared to uniform sampling. This strongly shortens the measurement time, a serious issue of EMC/EMI near-field investigations.

As future developments, let us stress that the approach can be extended to account for the features of the measurement probe [48, 50] and to the full 3D case, it can be employed to characterize other, partially coherent (e.g., quasi-homogeneous) sources and that the same concepts can be also applied to other application fields as, for example, the mapping of on-ground electromagnetic field [51]. Finally, the recent development of probe arrays can further provide an efficient means to drastically reduce time-consuming measurement procedures [52].

REFERENCES

1. Clayton, R. P., *Introduction to Electromagnetic Compatibility*, J. Wiley & Sons, Hoboken, NJ, 2006.
2. Fang, H., S. Changsheng, L. Deyun, and L. Guoding, "Measurement of radiated emission from PC computer system," *Proc. of the IEEE Int. Symp. on Electromag. Compat.*, 208–209, Cherry Hill, NJ, USA, Aug. 12–16, 1991.
3. Criel, S., L. Martens, and D. De Zutter, "Theoretical and experimental near-field characterization of perforated shields," *IEEE Trans. on Electromagn. Compat.*, Vol. 36, No. 3, 161–168, Aug. 1994.
4. Slattery, K. P., J. W. Neal, and W. Cui, "Near-field measurements of VLSI devices," *IEEE Trans. on Electromagn. Compat.*, Vol. 41, No. 4, 374–384, Nov. 1999.
5. Antonini, G., S. Cristina, and A. Orlandi, "EMC characterization of SMPS devices: Circuit and radiated emissions model," *IEEE Trans. on Electromagn. Compat.*, Vol. 38, No. 3, 300–309, Aug. 1996.
6. Beghou, L., B. Liu, L. Pichon, and F. Costa, "Synthesis of equivalent 3-D models from near field measurements application to the EMC of power printed circuit boards," *IEEE Trans. on Magn.*, Vol. 45, No. 3, 1650–1653, Mar. 2009.
7. De Daran, F., J. Chollet-Ricard, F. Lafon, and O. Maurice, "Prediction of the field radiated at one meter from PCB's and microprocessors from near EM field cartography," *Proc. of the IEEE Int. Symp. on Electromag. Compat.*, 479–482, Istanbul, Turkey, May 11–16, 2003.
8. Corona, P., J. Ladbury, and G. Latmiral, "Reverberation-chamber research-then and now: A review of early work

and comparison with current understanding," *IEEE Trans. on Electromag. Compat.*, Vol. 44, No. 1, 87–94, Feb. 2002.

9. Sreenivasiah, I., D. C. Chang, and M. T. Ma, "Emission characteristics of electrically small radiating sources from tests inside a TEM cell," *IEEE Trans. on Electromag. Compat.*, Vol. 23, No. 3, 113–121, Aug. 1981.
10. Koepke, G., D. Hill, and J. Ladbury, "Directivity of the test device in EMC measurements," *Proc. of the IEEE Int. Symp. on Electromag. Compat.*, 535–539, Washington, DC, USA, Aug. 21–25, 2000.
11. Bolomey, J. C., "Introduction to near-field techniques for EMC applications: State of the art and prospectives," *Proc. of the IEEE Int. Symp. on Electromag. Compat.*, 356, Montreal, CA, Aug. 13–17, 2001.
12. Regué, J.-R., M. Ribó, J. M. Garrell, and A. Martín, "A genetic algorithm based method for source identification and far-field radiated emissions prediction from near-field measurements for PCB characterization," *IEEE Trans. Electromagn. Compat.*, Vol. 43, No. 4, 520–530, Nov. 2001.
13. Baudry, D., C. Arcambal, A. Louis, B. Mazari, and P. Eudeline, "Applications of the near-field techniques in EMC investigations," *IEEE Trans. Electromagn. Compat.*, Vol. 49, No. 3, 485–493, Aug. 2007.
14. Manjombe, Y. T., Y. Azzouz, D. Baudry, B. Ravelo, and M. E. H. Benbouzid, "Experimental investigation on the power electronic transistor parameters influence to the near-field radiation for the EMC applications," *Progress In Electromagnetics Research M*, Vol. 21, 189–209, 2011.
15. Deschrijver, D., F. Vanhee, D. Pissoort, and T. Dhaene, "Automated near-field scanning algorithm for the EMC analysis of electronic devices," *IEEE Trans. Electromagn. Compat.*, Vol. 54, No. 3, 502–510, Jun. 2012.
16. Chevallier, D., D. Baudry, and A. Louis, "Development of an optical near-field test bench for EMC application," *Proc. of the Int. Symp. on Electromagn. Compat.*, 531–536, York, UK, Sep. 26–30, 2012.
17. Laurin, J. J., Z. Ouardhiri, and J. Colinas, "Near-field imaging of radiated emission sources on printed-circuit boards," *Proc. of the IEEE Int. Symp. on Electromagn. Compat.*, 368–373, Montreal, CA, Aug. 13–17, 2001.
18. Taaghol, A. and T. Sarkar, "Near-field to near/far-field transformation for arbitrary near-field geometry, utilizing an equivalent

magnetic current," *IEEE Trans. Electromagn. Compat.*, Vol. 38, No. 3, 536–542, Aug. 1996.

19. Capozzoli, A., C. Curcio, G. D'Elia, and A. Liseno, "Singular-value optimization in plane-polar near-field antenna characterization," *IEEE Antennas Prop. Mag.*, Vol. 52, No. 2, 103–112, Apr. 2010.
20. Yaghjian, A., "An overview of near-field antenna measurements," *IEEE Trans. Antennas Prop.*, Vol. 34, No. 1, 30–45, Jan. 1986.
21. Capozzoli, A., C. Curcio, A. Liseno, and P. Vinetti, "Field sampling and field reconstruction: A new perspective," *Radio Sci.*, Vol. 45, RS6004, 2010, doi:10.1029/2009RS004298.
22. Capozzoli, A., C. Curcio, and A. Liseno, "Multi-frequency planar near-field scanning by means of Singular-Value Decomposition (SVD) optimization," *IEEE Antennas Prop. Mag.*, Vol. 53, No. 6, 212–221, Dec. 2011.
23. Fourestié, B., Z. Altman, J. C. Bolomey, J. Wiart, and F. Brouaye, "Statistical modal analysis applied to near-field measurements of random emissions," *IEEE Trans. Antennas Prop.*, Vol. 50, No. 12, 1803–1812, Dec. 2002.
24. De Jongh, R. V., M. Hajian, and L. P. Ligthart, "Antenna time-domain techniques," *IEEE Trans. Antennas Prop.*, Vol. 39, No. 5, 7–12, Oct. 1997.
25. Capozzoli, A., C. Curcio, G. D'Elia, and A. Liseno, "Phaseless antenna characterization by effective aperture field and data representations," *IEEE Trans. Antennas Prop.*, Vol. 57, No. 1, 215–230, Jan. 2009.
26. Fourestié, B., J. C. Bolomey, T. Sarrebourse, Z. Altman, and J. Wiart, "Spherical near field facility for characterizing random emissions," *IEEE Trans. Antennas Prop.*, Vol. 53, No. 8, 2582–2589, Aug. 2005.
27. Gennarelli, C., M. Migliaccio, and C. Savarese, "On the interpolation of stochastic E. M. fields," *Proc. of the Antennas and Propagation Soc. Int. Symp.*, 1622–1625, Seattle, WA, Jun. 20–24, 1994.
28. LaHaie, I. J., "Inverse source problem for three-dimensional partially coherent sources and fields," *J. Opt. Soc. Am. A*, Vol. 2, No. 1, 35–45, Jan. 1985.
29. Goodman, J. W., *Introduction to Fourier Optics*, McGraw-Hill, San Francisco, CA, 1968.
30. Capozzoli, A., C. Curcio, A. Esposito, and A. Liseno, "Field sampling of incoherent sources," *Proc. of the Antennas and*

Propagation Soc. Int. Symp., 1646–1649, Spokane, WA, Jul. 3–8, 2011.

31. Jones, D. S. J., *Methods in Electromagnetic Wave Propagation*, IEEE Press, New York, NY, 1995.
32. Born, M. and E. Wolf, *Principles of Optics*, 7th Edition, Cambridge University Press, Cambridge, UK, 1999.
33. Devaney, A. J., "The inverse problem for random sources," *J. Math. Phys.*, Vol. 20, No. 8, 1687–1691, 1979.
34. Landau, H. J. and H. O. Pollak, "Prolate spheroidal wave functions, Fourier analysis and uncertainty III: The dimension of essentially time- and band-limited signals," *Bell Syst. Tech. J.*, Vol. 41, 1295–1336, Jul. 1962.
35. Marks, D. L., R. A. Stack, and D. J. Brady, "Three-dimensional coherence imaging in the Fresnel domain," *Appl. Opt.*, Vol. 38, No. 8, 1332–1342, Mar. 1999.
36. Collin, R. E., *Field Theory of Guided Waves*, IEEE Press, New York, 1991.
37. Hansen, T. B. and A. D. Yaghjian, "Planar near-field scanning in the time domain, Part 1: Formulation," *IEEE Trans. Antennas Prop.*, Vol. 42, No. 9, 1280–1291, Sep. 1994.
38. Harrington, R. F., *Time-harmonic Electromagnetic Fields*, IEEE Press, New York, 2001.
39. LaHaie, I. J., "Uniqueness of the inverse source problem for quasi-homogeneous, partially coherent sources," *J. Opt. Soc. Am. A*, Vol. 3, No. 7, 1073–1079, Jul. 1986.
40. Hoenders, B. J. and H. P. Baltes, "On the existence of non-radiating frequencies in the radiation from a stochastic current distribution," *J. Phys. A: Math. Gen.*, Vol. 13, No. 3, 995–1006, Mar. 1980.
41. Helstrom, C. W., "Modal decomposition of aperture fields in detection and estimation of incoherent objects," *J. Opt. Soc. Am.*, Vol. 60, No. 4, 521–530, Apr. 1970.
42. Twomey, S., "The application of numerical filtering to the solution of integral equations encountered in indirect sensing measurements," *J. Franklin Inst.*, Vol. 279, No. 2, 95–109, 1965.
43. Bertero, M. and P. Boccacci, *Introduction to Inverse Problems in Imaging*, Institute of Physics Publishing, Bristol, UK, 1998.
44. Gori, F. and G. Guattari, "Shannon number and degrees of freedom of an image," *Opt. Commun.*, Vol. 7, No. 2, 163–165, Feb. 1973.
45. Kildal, P. S. and K. Rosengren, "Correlation and capacity of

MIMO systems and mutual coupling, radiation efficiency, and diversity gain of their antennas: Simulations and measurements in a reverberation chamber," *IEEE Commun. Mag.*, Vol. 42, No. 12, 104–112, Dec. 2004.

46. Hill, D. A., "Plane wave integral representation for fields in reverberation chambers," *IEEE Trans. Electromagn. Compat.*, Vol. 40, No. 3, 209–217, Aug. 1998.
47. Rahmat-Samii, Y., V. Galindo-Israel, and R. Mittra, "A plane-polar approach for far-field construction from near-field measurements," *IEEE Trans. Antennas Prop.*, Vol. 28, No. 2, 216–230, Mar. 1980.
48. Capozzoli, A., C. Curcio, and A. Liseno, "Multi-frequency, multi-resolution and probe compensated advanced near-field antenna characterization," *Proc. of the Europ. Conf. on Antennas Prop.*, 2542–2546, Prague, Czech Republic, Mar. 26–30, 2012.
49. International Electrotechnical Commission (IEC), "CISPR 16: Specifications for radio disturbance and immunity measuring apparatus and methods," 2010.
50. Capozzoli, A., C. Curcio, G. D'Elia, F. Ferrara, C. Gennarelli, R. Guerriero, and A. Liseno, "A probe compensated helicoidal NF-FF transformation for aperture antennas using a prolate spheroidal expansion," *Int. J. of Antennas Prop.*, Vol. 2012, Article ID 753156, 13 pages, 2012, doi:10.1155/2012/753156.
51. Bucci, O. M., A. Capozzoli, G. D'Elia, and A. Liseno, "Mapping the electromagnetic field intensity at the ground: Analysis of an incoherent scene and extension to a partially coherent scenario," *Proc. of the XVI Riunione Nazionale di Elettromagnetismo*, 388–391, Genoa, Italy, Sep. 18–21, 2006.
52. "A new, non perturbing system, for the measurement of high frequency electromagnetic fields," National Coordinator: G. D'Elia, Progetto di Rilevante Interesse Nazionale, Research Program Funded by the Italian Ministry for University and Research, Apr. 2005.